Desalination and Water Treatment
www.deswater.com

doi: 10.5004/dwt.2022.28754

271 (2022) 232–243
September

Microwave-assisted rapid synthesis of Al-doped Fe_3O_4/hydroxyapatite magnetic nanocomposites in pectin matrix for removal of fluoride from aqueous solution

Dezhi Qin[a], Guangrui Yang[b], Li Zhang[a,*]

[a]*College of Chemistry and Environmental Engineering, Pingdingshan University, Pingdingshan 467000, China, emails: lizhangpds@126.com (L. Zhang), dezhiqin@163.com (D. Qin)*
[b]*Institute of Environmental and Municipal Engineering, North China University of Water Resources and Electric Power, Zhengzhou 450011, China, email: guangruiyang1208@163.com (G. Yang)*

Received 27 January 2022; Accepted 14 July 2022

ABSTRACT

The Al-doped Fe_3O_4/hydroxyapatite (HAP) nanocomposites prepared in pectin matrix was employed as adsorbent that offers high adsorption capacity for fluoride, magnetic separability and good stability. Powder X-ray diffraction and transmission electron microscopy characterizations were used to determine the structure and morphology of as-prepared samples. The needle-like Al-doped Fe_3O_4/HAP nanocrystals were coated with pectin molecules, which not only induced the nucleation, but inhibited the further growth of nanocrystals. The results of thermogravimetric analysis and Fourier transform infrared spectra showed that the obtained products are organic–inorganic nanocomposites; and the Al doping in composites increased the amount of hydroxyl groups, which could supply more adsorption sites for fluoride. In bath experiments, the adsorption capacity of Al-doped samples was significantly higher than that of pure HAP due to the high affinity of aluminium toward fluoride. The effect of reaction parameters such as pH, calcination temperature, co-existing anions and Al/Ca molar ratio on the adsorption capacity was also investigated to determine optimum adsorption condition. The Al-doped Fe_3O_4/HAP nanocrystals exhibited high adsorption rate for fluoride during the first 30 min and reached equilibrium within 80 min. The adsorption kinetics and isotherms were well-fitted by the pseudo-second-order kinetic model and the Freundlich isotherm model, respectively. In addition, the adsorption mechanism of fluoride on Al-doped Fe_3O_4/HAP nanocomposites was investigated, which can be mainly attributed to electrostatic attraction and ion-exchange.

Keywords: Al doping; Fluoride adsorption; Hydroxyapatite; Magnetic materials; Nanocomposites; Polysaccharide-assisted synthesis

1. Introduction

As essential micronutrient for human health, fluoride is usually ingested through food and drinking water. However, excess ingestion of fluoride can cause a series of diseases such as skeletal and dental fluorosis, muscle fibre degeneration, skin rashes, even neurological damage [1,2]. The World Health Organization (WHO) recommends that the maximum acceptable concentration of fluoride in drinking water should not exceed 1.5 mg/L. Up to now fluoride contamination in drinking water possesses a great risk to millions of people in many regions of the world, especially in North Africa, China and India [2]. For this reason, different technologies have been adopted to abate excess fluoride

* Corresponding author.

from aqueous solution, including adsorption, ion exchange, precipitation, and membrane filtration [3–5]. Among these methods, adsorption is an economical and effective methods for removing fluoride from the water without generation of hazardous by-products [6,7].

To date, various materials have been as adsorbents for the treatment of pollutants in water, such as activated carbon, zeolite, biomass, mesoporous silica, clay and hydroxyapatite [8–12]. Hydroxyapatite has been considered to be an attractive absorbent for removal of heavy metal and dyes from aqueous solution on account of its biocompatibility, low water solubility, low cost and high stability [13–15]. For example, Si et al. synthesized porous HAP nanoparticles with a large surface area by hydrothermal method, and the as-prepared HAP nanoparticles exhibited high adsorption capacities for the Cr(III), Pb(II) and Cu(II) ions [16]. Moreover, much interest has focused on producing and improving adsorption performance of hydroxyapatite by doping with impurities in recent years [14,17]. The doping of metal ions in HAP often possesses unique structure and property due to complementary or synergistic effects, leading to significantly enhanced adsorption performance. Some substituting cations like Mg, La, Al, Na and Fe can be easily induced into the apatite crystal lattice, which increased the content of hydroxyl group of HAP, and thus improved adsorption capacity with fluoride ions [14,17–19]. Based on pertinent reports, it has been acknowledged that Al ion as hard acid has a high affinity to fluoride (hard base), which benefits the fluoride adsorption. For example, the study by Chen et al. showed that defluoridation capacity of Al-doped hydroxyapatite was larger than that of La and Mg-doped hydroxyapatite [17]. Liu et al. reported the synthesis of a biocompatible Al-HAP adsorption membrane for rapid removal of fluoride from aqueous solution [20]. The major limitations for large scale application of hydroxyapatite-based adsorbents are its powder form and insufficient strength, which results in high turbidity, difficulty in separation from aqueous and low recovery. The use of magnetic nanoparticles, easily recovered from solution by an external magnetic field, offers a good way to remediate this problem. Recent studies showed that Fe_3O_4 magnetic nanoparticles can be hybridized with adsorbents to facilitate the recovery of the adsorbents from aqueous solution [21,22]. The presence of ferroferric oxide in nanocomposites leads to the absorbent can be easily separated and reused by an external magnetic field, which also avoids the secondary pollution caused by adsorbents.

Different synthetic methods have been developed for the size- and shape-controlled synthesis of hydroxyapatite nanocrystals, such as sol-gel processing, chemical bath deposition, hydrothermal/ solvothermal methods. However, these methods have some disadvantages involving harsh reaction conditions, requirement of toxic organic solvents or ligands. Recently, to eliminate the use of toxic organic solvents, biomolecules such as polysaccharides, amino acids, peptides, proteins and other eco-friendly biological agents were chosen as templates to synthesize shape and size-controllable inorganic nanomaterials because of their multiple functional groups, specific geometrical configuration, and electronic structure [23,24]. Moreover, these hybrid nanocomposites offer the dual advantages of inorganic and organic materials like rigidity, thermal stability, flexibility and processability. The pectin is a water-soluble polysaccharide existing in most plants cell wall, which has been widely used in the biomedical fields, such as drug delivery, tissue engineering, and bone repairing due to its biocompatibility, low cost and easy availability [25]. In some cases of biosynthesis, pectin was used as matrix to stabilize and modify inorganic nanomaterials to remove pollutants [26,27]. For example, stable water-soluble pectin-Ag (0) nanobiocomposites were prepared by using a pectinic polysaccharide as matrix isolated from bark, in which the coatings are formed through the binding of the pectin polymer chains and Ag nanoparticles into a complex with non-covalent interactions [28].

Herein, we report a facile microwave-assisted method for the preparation of Al-doped Fe_3O_4/hydroxyapatite magnetic nanocomposites in pectin matrix. The as-prepared nanocomposites were investigated as adsorbent for removing fluoride from aqueous solution. Microwave-assisted synthesis has the advantages of short reaction time, small particle size and high purity of prepared samples, and the resulting products are more uniform in terms of size and composition. The effects of adsorption time, pH value, calcination temperature, co-existing anions and Al/Ca molar ratio on the performance of defluoridation were examined. In general, the goal of this study is to develop a biocompatible, low cost and efficient magnetic nanocomposite adsorbent with high adsorption capacity for fluoride in water.

2. Materials and methods

2.1. Materials

Pectin (galacturonic acid dry basis ≥ 74%), NaF and $Al_2(SO_4)_3{\cdot}18H_2O$ were purchased from Aladdin Chemical Reagent Company. $FeCl_3{\cdot}6H_2O$, $FeCl_2{\cdot}4H_2O$, $CaCl_2$ and $(NH_4)_2HPO_4$ were purchased from Sinopharm Chemical Regent Company. All chemicals were of analytical reagent grade and can be used without further purification. Deionized and doubly distilled water with a resistivity of 18.25 MΩ·cm was used throughout this work.

2.2. Preparation of Al-doped Fe_3O_4/HAP magnetic nanocomposites

Al-doped Fe_3O_4/HAP nanocomposites were synthesized in pectin matrix by a simple microwave-assisted method. In a typical experimental procedure, 0.54 g of $FeCl_3{\cdot}6H_2O$ and 0.20 g of $FeCl_2{\cdot}4H_2O$ were dissolved in 200 mL of pectin solution (10 g/L) with vigorous stirring under N_2 protection, and the pH value was adjusted to 11 by addition of 2 mol/L of NaOH. The mixed solution was rapidly microwave-heated in the microwave reaction system (2450 MHz, 400 W) for 5 min. Then, the reaction solution was maintained at 90°C for 1 h, and cooled down to room temperature naturally. The obtained Fe_3O_4 nanocrystals were washed several times with water and ethanol, freeze-dried at –4°C for further use.

For the synthesis of Al-doped Fe_3O_4/HAP nanocomposites, 0.555 g of $CaCl_2$ was dissolved in 100 mL of pectin solution (10 g/L), and the mixed solution was shaken for 1 h

to obtain pectin-Ca^{2+} homogeneous emulsion. 0.289 g of Fe_3O_4 was added into the above solution with ultrasonic treatment for 5 min. Subsequently, 0.395 g of $(NH_4)_2HPO_4$ (Ca/P molar ratio = 1.67) was dissolved in 100 mL of pectin solution (10 g/L) and slowly added into as-prepared pectin-Fe_3O_4/Ca^{2+} solution with vigorous stirring at room temperature. In this process, the pH value of the solution was maintained at about 10 adjusting by 10% of NaOH solution. Then, the reaction system was heated for 15 min by microwave (2450 MHz, 240 W). After the reaction completed, 20 mL of freshly prepared $Al_2(SO_4)_3$ solution was injected pectin-Fe_3O_4/HAP emulsion with vigorous stirring, and the pH value was adjusted to about 7. Finally, the mixed solution was located on a microwave system (2450 MHz) and heated at 240 W for 12 min. The obtained products were separated by high-speed centrifuging at 12,000 rpm, and dried at 60°C in vacuum for 36 h.

2.3. Batch adsorption experiments

A stock solution of fluoride (1,000 mg/L) was prepared by dissolving appropriate amount of NaF in double distilled water. The experimental solution was obtained by diluting the stock solution with deionized water to the desired initial fluoride concentration. All the bath adsorption experiments were carried out in a thermostated shaker with a shaking speed of 100 rpm using 100 mL polyethylene vials. The 50 mL of fluoride solution with different concentrations and 0.05 g adsorbent were filled with vials and placed in water bath to shake at certain time intervals and temperatures. At the end of the adsorption process, adsorbent was separated from the solution by magnet; and the solution was filtered using microporous filter membrane. The concentration of fluoride left in the supernatant was determined with a fluoride-selective electrode (PF-101, Rex Electric Chemical) by using TISAB buffer solution to adjust total ionic strength.

The amount of fluoride at equilibrium q_e (mg/g) on the adsorbent samples was calculated from the following equation:

$$q_e = \frac{(C_0 - C_e)V}{m} \quad (1)$$

where c_0 and c_e (mg/L) are the fluoride concentrations at initial and equilibrium, respectively; V (L) is the volume of the solution and m (g) is the mass of adsorbents.

2.4. Characterization techniques

Powder X-ray diffraction (XRD) characterization was carried out on a Rigaku Smartlab diffractometer. Transmission electron microscopy (TEM) and energy-dispersive X-ray spectrum (EDX) were acquired on a JEOL JEL-2010 transmission electron microscope equipped with an X-ray energy-dispersive detector. Thermogravimetric analysis (TGA) was performed on a TA Q-600 thermogravimetric apparatus. Aluminium residual concentration was determined by inductively coupled plasma optical emission spectrometer (ICP-OES, Agilent 725ES). Fourier transform infrared (FT-IR) spectra were collected on a Bruker Tensor-37 spectrophotometer in the wave number range of 4,000–400 cm^{-1}. Surface charges of adsorbents were measured by a laser Doppler velocimetry (Malvern NanoZS-90).

3. Results and discussion

Fig. 1a shows the XRD patterns of pectin modified Fe_3O_4, Fe_3O_4/HAP and Al-doped Fe_3O_4/HAP nanocomposites. The low intensity and broadening of the XRD peaks are due to the very small size of the as-prepared nanocomposites. The major diffraction peaks at 2θ of 31.34°, 35.45°, 43.18°, 53.98°, 56.71° and 63.39° can be respectively indexed to (220), (311), (400), (422), (511) and (440) crystal planes of Fe_3O_4 with spinel structure. As shown in XRD pattern of Fe_3O_4/HAP, the 2θ peaks at about 25.93° (002) and 32.11° (211) are assigned to characteristic peaks of HAP. The Ca/P molar ratio determined by ICP-OES analysis is 1.64, which is close to 1.67 for stoichiometric HAP, indicating the formation of HAP. EDX spectrum (Fig. 1b) result shows that the existence of Al, Ca, P, Fe in nanocomposites, note that Cu-related peaks come from the TEM grids. However, the Bragg reflections corresponding to $Al(OH)_3$ are not observed in the XRD pattern of Al doped Fe_3O_4/HAP nanocomposites, which suggests the amorphous nature of the $Al(OH)_3$. ICP-OES analysis shows that the Ca/P molar ratio (1.48) of Al doped Fe_3O_4/HAP is lower than that of HAP, confirming the replacement of Ca with Al ions.

The morphology of pectin-conjugated Al-Fe_3O_4/HAP nanocrystals was depicted by TEM measurement. Fig. 2a is the TEM image of pectin-Fe_3O_4 nanocrystals, clearly showing that the nanoparticles are approximately spherical in shape with size at about 3~6 nm. Some Fe_3O_4 particles are prone to aggregation and grow to form larger clusters/nanoparticles (15~25 nm), and these nanoparticles are well dispersed from each other due to the surface modification by pectin molecules. Fig. 2b shows a representative TEM image of Al-doped Fe_3O_4/HAP nanocrystals in the pectin solution from the typical experiment. From the figure, these nanocrystals are needle-like morphology with about 150~300 nm in length and 10~20 nm in width. The HRTEM image in Fig. 2c provides further insight into the structure of the as-prepared products. It reveals that many Fe_3O_4 nanoparticles exist on the inside of HAP, which guarantees the magnetic properties of the samples. The HRTEM image looks fuzzy and well-defined crystal lattice is not observed, suggesting the surface coating of samples by pectin film. To investigate the influence of pectin on the formation of Al-doped Fe_3O_4/HAP nanocomposites, control experiment was carried out in the aqueous solution without pectin. As shown in Fig. 2d, it is becoming clear that obvious aggregation is associated with the absence of pectin, which is unfavorable for the adsorption of fluoride because of smaller specific surface areas. It was suggested by Ribeiro et al. [29] that the long-chain structure of pectin molecules containing hydroxyl-, ester-, carboxylate- and amine groups can act as surface ligands interacting with the surface of nanocrystals to control the size and morphology. The TGA characterization also confirmed the existence of pectin in Al-doped Fe_3O_4/HAP nanocomposites. There are three stages of weight loss in TGA curve (Fig. 2e) of as-prepared products. The first stage of the decomposition

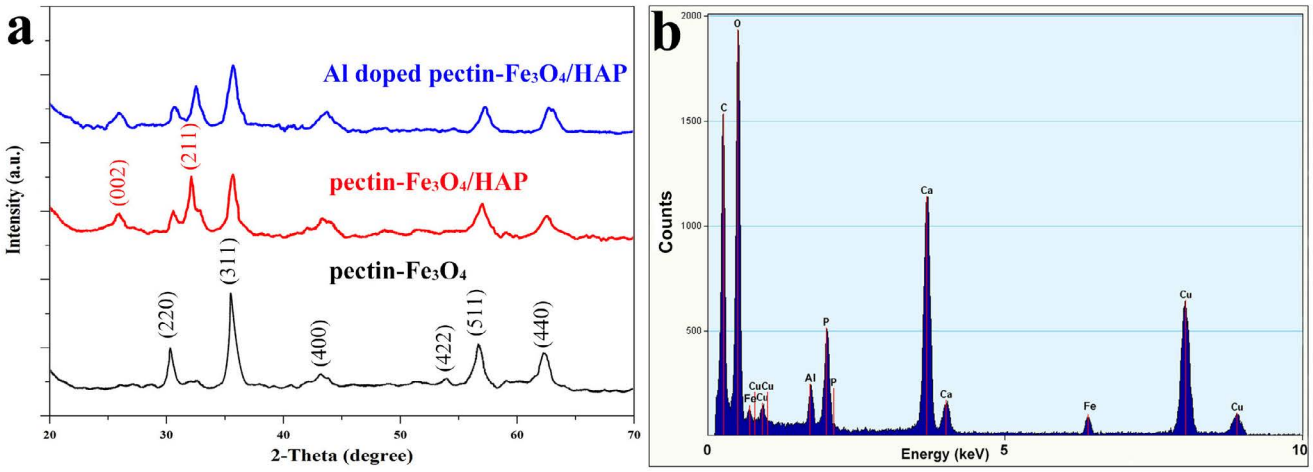

Fig. 1. (a) XRD patterns of pectin-Fe_3O_4, pectin-Fe_3O_4/HAP and Al-doped Fe_3O_4/HAP (Al/Ca molar ratio = 1:4) and (b) EDX spectrum of Al-doped Fe_3O_4/HAP (Al/Ca molar ratio = 1:4).

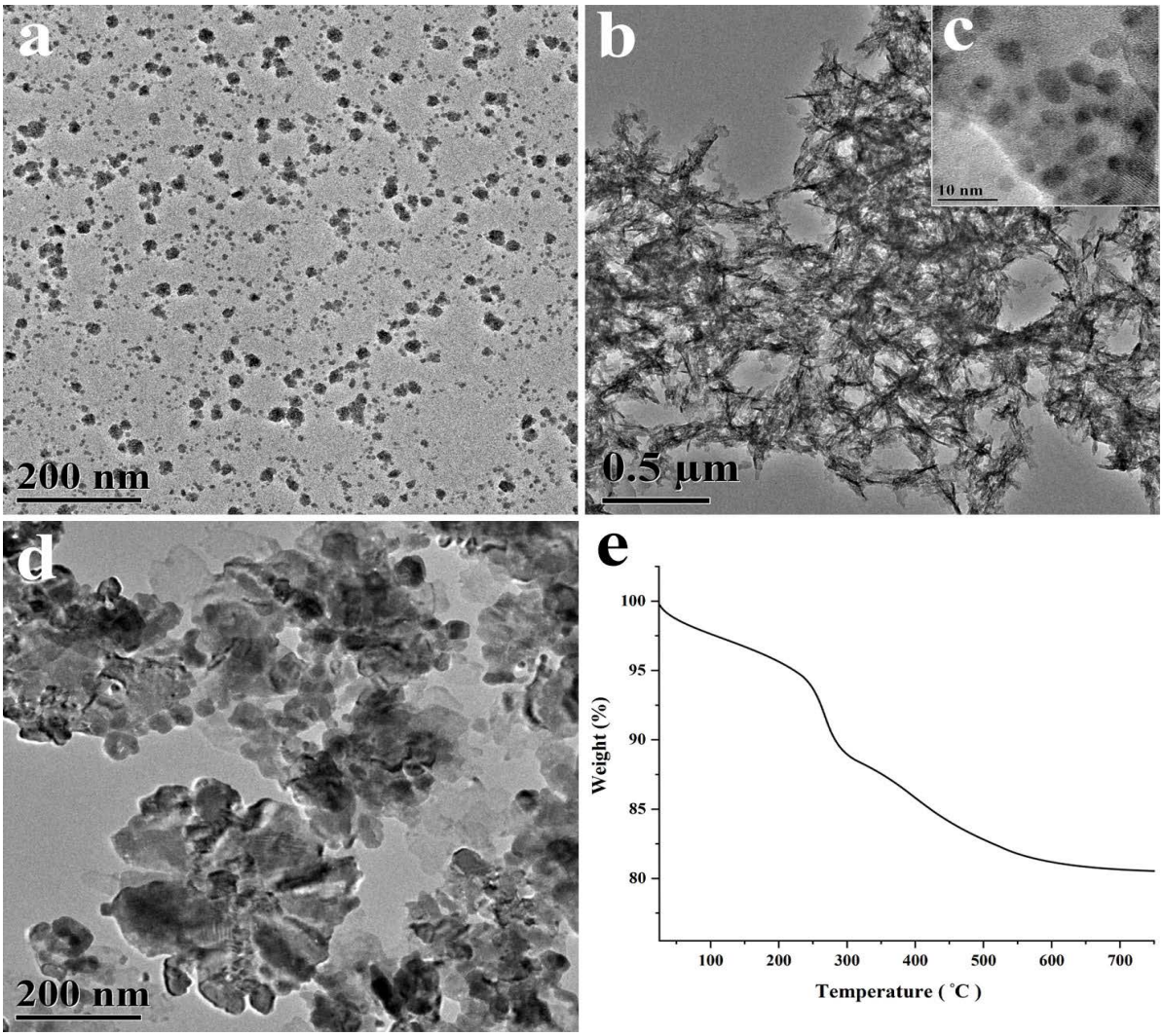

Fig. 2. (a) TEM image of pectin-Fe_3O_4 nanocrystals, (b) TEM and (c) HRTEM images of Al-doped pectin-Fe_3O_4/HAP nanocrystals (Al/Ca molar ratio = 1:4), (d) TEM image of Al-doped Fe_3O_4/HAP prepared in the absence of pectin, and (e) TGA curve of Al-doped pectin-Fe_3O_4/HAP nanocrystals (Al/Ca molar ratio = 1:4).

observed up to 225°C is due to moisture evaporation. From 225°C to 270°C, the loss of weight is mainly owing to the dehydration process of aluminium hydroxide. The third stage of the decomposition is observed from 270°C to 600°C corresponding to the pyrolysis of pectin molecules, indicating that the obtained products are inorganic-organic hybrid materials.

Fig. 3a–c show the FT-IR spectra of pectin-Fe_3O_4/HAP nanocrystals, Al-doped and fluoride-loaded the as-prepared samples, respectively. As can be seen in IR spectra, the IR bands at about 2,936; 1,736; 1,638; 1,395 cm^{-1} should be mainly attributed to C–H, C=O in free carboxylic acid and carboxylate (COO−) groups of pectin molecules, respectively; the appearance of the peaks at 1,090; 1,036; 962; 600 and 470 cm^{-1} indicates the formation of the apatite phase. The IR peaks at 582 and 565 cm^{-1} are assigned to stretching vibration of Fe–O, which confirms the successful combination of HAP with Fe_3O_4. The existence of magnetic material in composites is easy to realize the solid–liquid separation after adsorption. In IR spectrum of pectin-Fe_3O_4/HAP (Fig. 3a), the peaks of 3,565 and 1,456 cm^{-1} are attributed to O–H and CO_3^{2-} groups. In Fig. 3b, an additional IR peak at 907 cm^{-1} attributed to O–Al–O is observed by the doping of Al ions in matrix. Compared with the IR spectrum of Fe_3O_4/HAP (Fig. 3a), the intensity of IR peaks ascribing CO_3^{2-} groups obviously weakens and the characteristic peak for the O–H stretching vibration is enhanced and blue-shifted (Fig. 3b). Obviously, the doping of Al in samples increased the content of hydroxyl group of hydroxyapatites, which could supply more ion-exchange sites for fluoride. Conversely, the IR peak of hydroxyl groups weakens again in fluoride-loaded adsorbents (Fig. 3c), which indicates that the fluoride ions has been incorporated into the HAP nanocrystalline and the hydroxyl groups on the surface might be replaced by fluoride ions.

Relative studies illustrated that self-organized porous architecture of adsorbents could be formed during calcination, which might be beneficial to adsorption application because more active adsorption sites are available for adsorbents [19,30]. Fig. 4a compares the adsorption of Al-doped Fe_3O_4/HAP nanocrystals at different calcination temperatures. It is evident that calcination temperature has less of effect on the fluoride adsorption, even slightly lower adsorption capacity with elevated temperature. Fig. 4b shows the TEM image of calcined Al-doped Fe_3O_4/HAP nanocrystals at 400°C. It can be seen that the particle size increases significantly and appears agglomerated with change in morphology on calcination; needle-like nanocrystals are beginning to gather and transform to bundle-like structures as indicated by the arrows in TEM picture. The above TGA analysis showed that the temperature for thermal depolymerization of pectin chains in composites is about 270°C. Therefore, the size and morphology of Al-doped Fe_3O_4/HAP nanocrystals changed after calcination without the protection of pectin matrix, which resulted in the decrease of adsorption capacity.

The effect of Al doping dose on the adsorption capacity of adsorbents was evaluated following the increase of Al/Ca molar ratio. As shown in Fig. 4c, an increased tendency of adsorption capacity was observed when the Al/Ca molar ratio was varied from 1:10 to 1:3. Al as a hard Lewis acid has well-known high affinity toward fluoride,

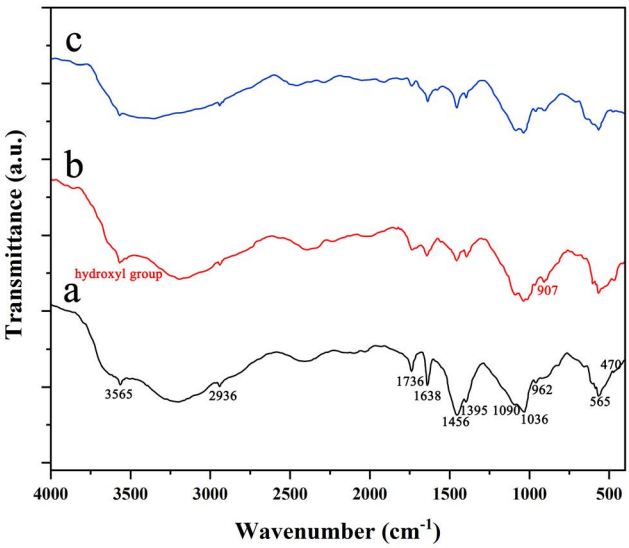

Fig. 3. FT-IR spectra of (a) pectin-Fe_3O_4/HAP nanocrystals, (b) Al-doped pectin-Fe_3O_4/HAP nanocrystals (Al/Ca molar ratio = 1:4), and (c) fluoride-loaded the as-prepared sample.

and has been use as cost efficient adsorbents for defluoridation treatment with good results [31]. Furthermore, the results of zeta potentials analysis showed that the positive charge of adsorbents increased after Al doping at different pH values, which was in favour of fluoride adsorption because of electrostatic attraction. However, excessive dose of Al doping might result in the increase of dissolution of Al ions in the water during the process of defluoridation. Al accumulates in human organs may cause severe nervous system diseases, and the WHO (1984) has recommended 0.2 mg/L as a guide line limit of Al ions in drinking water. The concentration of Al ions in solution after the fluoride adsorption experiments was measured using ICP-OES analysis to confirm the degree of dissolution. As illustrated in Fig. 4d, the amount of aluminium leaching in solution increased with the increase of Al/Ca molar ratio. As Al/Ca molar ratio was above 1:4, the concentration of Al ions in solution was close to the safe limit (0.2 mg/L) in drinking water. Thus, the molar ratio of Al to Ca 1:4 exhibited the higher efficiency for fluoride removal and was not harmful to water environment, which was used for the present adsorption experiments.

The pH of the solution is one of the important factors which significantly affect the extent of adsorption of fluoride. Fig. 5a shows the effect of the initial solution pH on the fluoride adsorption onto Al-doped Fe_3O_4/HAP nanocrystals at given conditions. Obviously, the maximum adsorption capacity is recorded at pH = 5 and shows gradual decreasing trend with increase and decrease of solution pH value. Results of Al-doped Fe_3O_4/HAP zeta potential at different pH values ranging from 3~11 (Fig. 5b) elucidated that the isoelectric point of the adsorbent was about 8.4. Compared with Fe_3O_4/HAP, the doping of Al resulted in the larger isoelectric point value, which indicates that the adsorbents are positively charged at a broader pH range and thus benefits the adsorption of negatively charged anions. Similar results were also reported by He et al. [20]. The surface

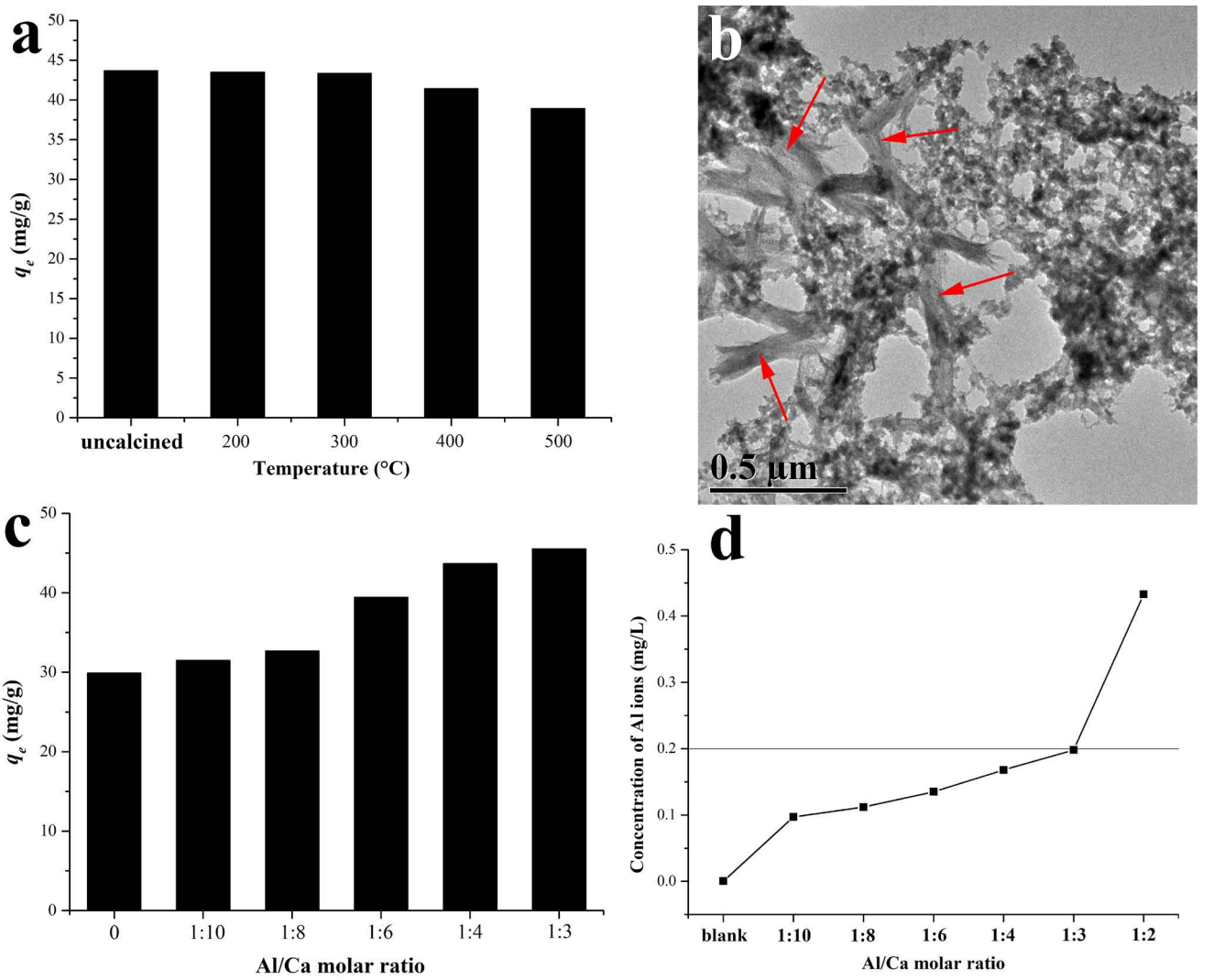

Fig. 4. (a) Effect of calcination temperature on fluoride adsorption capacity, (b) TEM image of calcined Al-doped Fe_3O_4/HAP nanocrystals at 400°C, (c) effect of Al doping dose on fluoride adsorption capacity, and (d) Al residual concentration in solution at different Al/Ca molar ratio.

of adsorbents is positively charged when the pH value is below the isoelectric point, and the electrostatic interaction between Al-doped Fe_3O_4/HAP nanocrystals and fluoride ions further promoted fluoride adsorption. Low adsorption capacity at pH < 4 could be attributed to the formation hydrofluoric acid, which reduced the electrostatic attraction between fluoride and the surface of adsorbents. Besides, hydroxyapatite is not stable under acidic condition and hence exhibited poor fluoride removal efficiency. The reduction of fluoride removal in alkaline condition is ascribed to electrostatic repulsion and the competition of hydroxyl with fluoride for adsorption sites because of similarity in charge and ionic radius [32]. The formation of $NaAlO_2$ at high pH values is also regarded as a reason for poor fluoride removal efficiency [20]. Although the optimum pH value for fluoride adsorption is about 5, adsorbents had a higher capacity to adsorb fluoride at a wider pH range (4~9). In present study, neutral condition (pH = 7) was selected as experimental factor because that it is near environmentally relevant pH range without the need for additional pH regulation. Moreover, low pH value may to a certain extent cause the dissolution of Al, Fe and Ca in water and bring toxic effect to environment.

Usually, there are several other co-existing anions along with fluoride at natural water, which may compete with fluoride at the adsorption sites of Al-doped Fe_3O_4/HAP nanocrystals. To explore the influence of anions on the adsorption capacity of adsorbents, six anions including Cl^-, NO_3^-, SO_4^{2-}, HCO_3^-, CO_3^{2-} and PO_4^{3-} with different concentrations were added into 50 mL of blank solution containing 0.05 g adsorbents and fluoride (100 mg/L), and then adsorption capacity was calculated in the control experiments, as shown in Fig. 6. The results revealed that the effect of Cl^-, NO_3^- and SO_4^{2-} on the adsorption of fluoride was considerably insignificant, even high concentration of Cl^- could enhance the adsorption capacity of adsorbents. The hydrolysis of HCO_3^-, CO_3^{2-} and PO_4^{3-} anions could produce OH-, and pH value of solution increased, which significantly

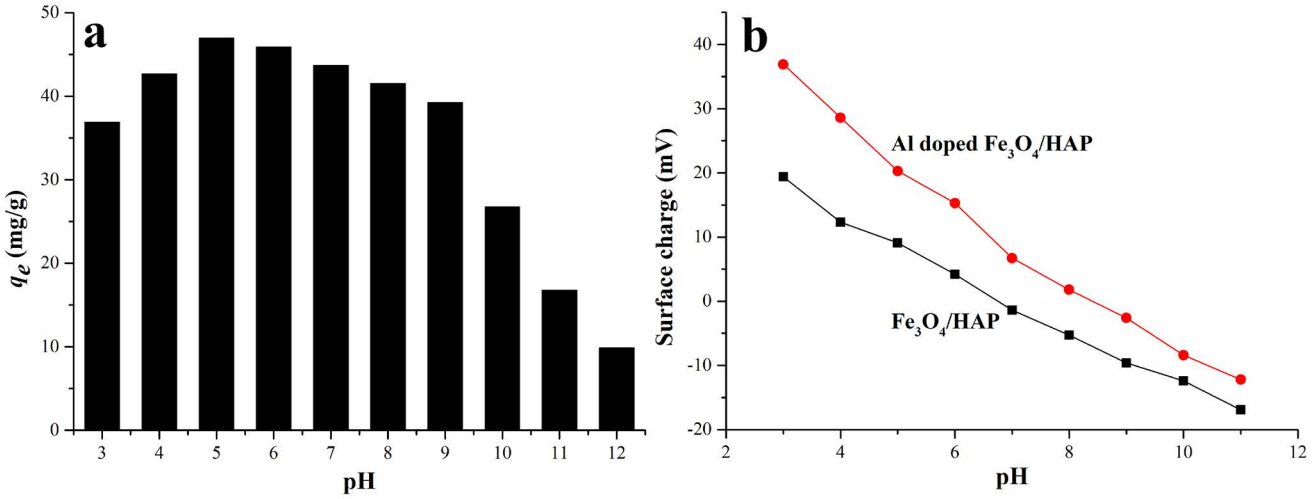

Fig. 5. (a) Effect of pH values on fluoride adsorption capacity (fluoride concentration = 100 mg/L, T = 45°C, V = 50 mL, adsorbent dose = 0.05 g) and (b) surface charges of Fe_3O_4/HAP and Al doped Fe_3O_4/HAP at different pH values.

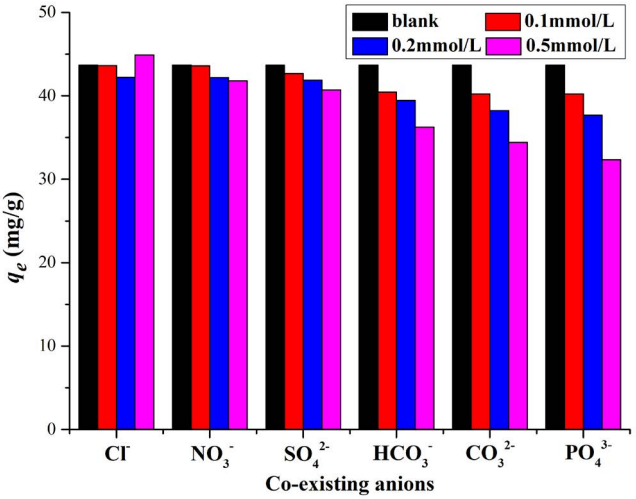

Fig. 6. Effect of co-existing anions on fluoride adsorption capacity.

reduced adsorption capacity of adsorbents. Similar results were reported by He et al. [20].

Adsorption kinetics is crucial in adsorption investigation because it can predict the adsorption removal rate of fluoride from aqueous solutions. Fig. 7a depicts the adsorption kinetics of fluoride on the Al-doped Fe_3O_4/HAP nanocrystals (Al/Ca molar ratio = 1:4) at different temperatures with an initial fluoride concentration of 100 mg/L (pH = 7). For fluoride adsorption, the removal efficiency increased sharply within 30 min and reached equilibrium at 80 min. This phenomenon is attributed to the high aqueous fluoride concentration and to a great deal of adsorption sites on the surface of adsorbents initially, causing fluoride to rapidly bind onto the adsorbent surface. Afterward, the active sites were gradually exhausted with the increase of contact time; the adsorption rate became slower and finally reached equilibrium. As shown in Fig. 7b, the pH value of solution gradually increased with adsorption time lasting. The fluoride ions could be adsorbed on the surface of the hydroxyapatite through the substitution of hydroxyl group owing to similarity in charge and ionic radius, and thereby caused the increase of pH value, which is consistent with the results of FT-IR analysis.

To further quantify the efficiency of fluoride adsorption with contact time, pseudo-first-order and pseudo-second-order kinetic models were employed to simulate and analyse the kinetic data, whose formulas are defined as follows:

$$\ln\left(q_e - q_t\right) = \ln q_e - k_1 t \tag{2}$$

$$\frac{t}{q_t} = \frac{1}{k_2 q_e^2} + \frac{t}{q_e} \tag{3}$$

where q_e and q_t (mg/g) are the equilibrium adsorption capacity and the amount of fluoride adsorbed at time t (min); k_1 (min^{-1}) and k_2 (g/mg min) are the pseudo-first-order, pseudo-second-order rate constants, respectively. The linear fitting plots and relevant calculated values of the pseudo-first-order and pseudo-second-order models at different temperatures are shown in Fig. 8 and Table 1. Obviously, the linear fitting plot of the pseudo-first-order kinetic model are not well aligned with the experimental data, showing R^2 value of less than 0.99. However, the pseudo-second-order kinetic model shows a good linear correlation with a R^2 value of nearly 1, and the calculated equilibrium adsorption capacity ($q_{e,calc}$) is in close agreement with the experimental values. The well-fitting to pseudo-second-order kinetic model suggests a chemisorption process involving ion exchange on the surface of Al-doped Fe_3O_4/HAP nanocrystals [33].

For a solid-liquid sorption process, the solute transfer is usually characterized by intraparticle diffusion control. The rate of intraparticle diffusion is a function of $t^{1/2}$ and can be defined as follows:

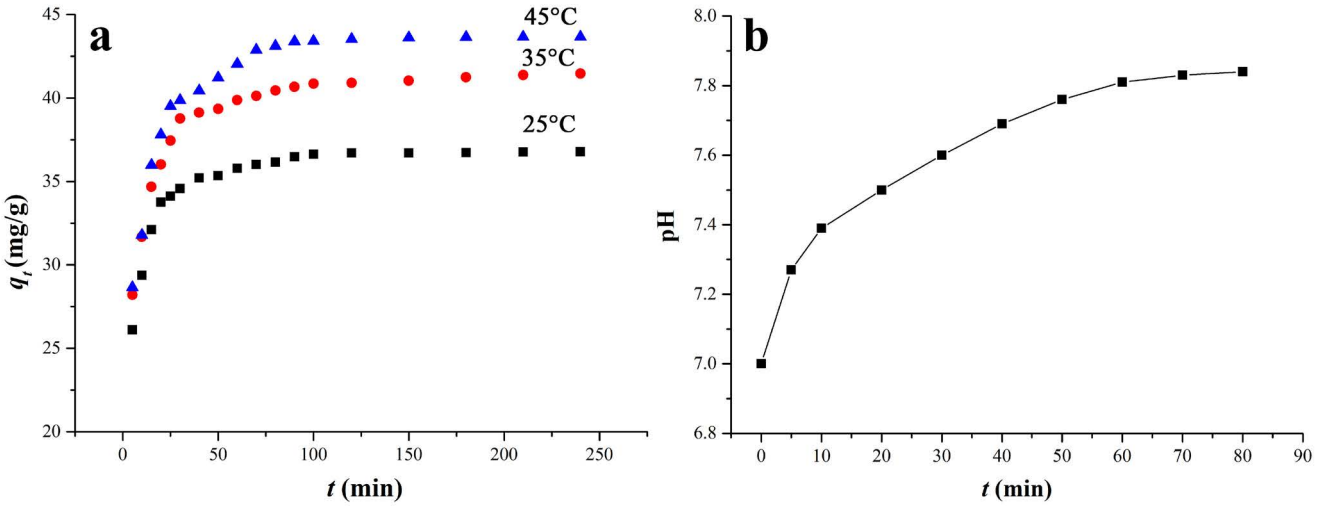

Fig. 7. (a) Adsorption kinetic of fluoride on the Al-doped pectin-Fe_3O_4/HAP nanocrystals at different temperatures (pH = 7, Al/Ca molar ratio = 1:4) and (b) pH change of fluoride solution with the increase of adsorption time (25°C).

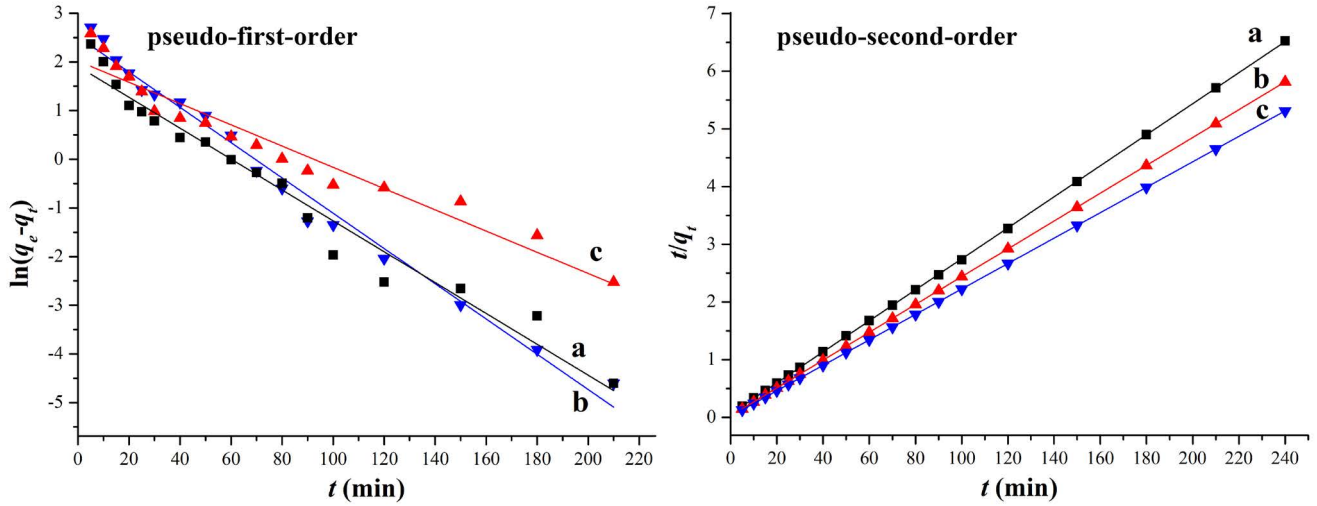

Fig. 8. Pseudo-first-order and pseudo-second-order plots for fluoride adsorption on Al-doped Fe_3O_4/HAP nanocrystals (a) 25°C, (b) 35°C and (c) 45°C.

Table 1
Rate constants and correlation coefficients of pseudo-first-order and pseudo-second-order kinetic models

Temperature	$q_{e,exp}$ (mg/g)	Pseudo-first-order			Pseudo-second-order		
		$q_{e,calc}$ (mg/g)	k_1 (min^{-1})	R^2	$q_{e,calc}$ (mg/g)	k_2 (g/mg min)	R^2
25°C	36.78	6.74	0.0317	0.9651	37.20	0.0122	0.9999
35°C	41.46	7.51	0.0218	0.9410	41.46	0.0220	0.9999
45°C	43.67	12.38	0.0362	0.9855	45.35	0.0250	0.9999

$$q_t = k_p t^{1/2} + C \quad (4)$$

where k_p (mg/g $min^{1/2}$) is the intraparticle diffusion rate constants, and C provides an idea of the boundary layer thickness. The k_p and C values can be obtained from the slope and intercept of the plot of q_t against $t^{1/2}$. Fig. 9 presents a linear fit of intraparticle diffusion model for adsorption of fluoride on Al-doped Fe_3O_4/HAP nanocrystals at different temperatures. As can be seen in figure, the fitted lines do not pass through the origin, which suggests that the intraparticle diffusion is not the only rate-limiting step.

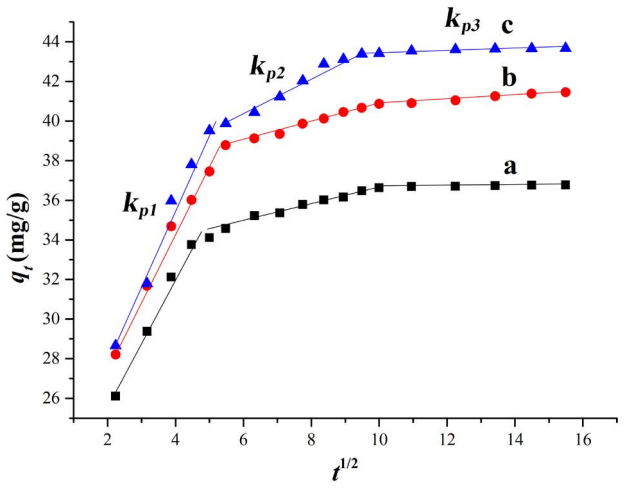

Fig. 9. Intraparticle diffusion plots for the adsorption of fluoride on Al-doped Fe_3O_4/HAP nanocrystals at different temperatures (a) 25°C, (b) 35°C and (c) 45°C.

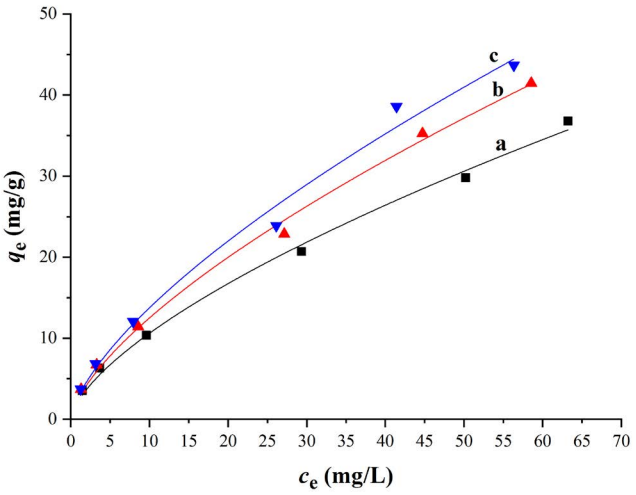

Fig. 10. Adsorption isotherms for fluoride on Al-doped Fe_3O_4/HAP nanocrystals (pH = 7, Al/Ca molar ratio = 1:4) (a) 25°C, (b) 35°C and (c) 45°C.

Moreover, three different linearity regions are observed over the entire period of contact time, indicating that three independent steps took place during the adsorption of fluoride on Al-doped Fe_3O_4/HAP nanocrystals. The first step represents the boundary layer diffusion while the following linear portion attributes to intraparticle diffusion, and the third step is the adsorption equilibrium stage [34]. Therefore, it can be concluded the adsorption process was complex and both external and intraparticle diffusion contribute to the rate of fluoride removal.

Fig. 10 shows adsorption isotherms for fluoride on Al-doped Fe_3O_4/HAP (Al/Ca molar ratio = 1:4) nanocrystals at pH = 7 and 25°C~45°C. The results revealed that the as-prepared samples exhibited good adsorption capacity for fluoride. It also can be seen that the q_e value increased with increasing the initial fluoride concentration, attributed to the relatively strong driving force of the concentration gradient at high initial concentrations. The increase of temperature favoured fluoride adsorption, suggesting an endothermic process. Two classic equilibrium isotherm models, that is, Langmuir and Freundlich were selected to fit the isotherm data. The Langmuir model assumes that no interaction occurs among adsorbate molecules, and that the adsorption is a monolayer. In contrast, the Freundlich model is employed to describe heterogeneous systems and reversible adsorption, which is not restricted to monolayer formations. The linear equations of Langmuir and Freundlich isotherm are expressed as follows:

$$\frac{C_e}{q_e} = \frac{C_e}{q_m} + \frac{1}{K_L q_m} \tag{5}$$

$$\ln q_e = \ln K_F + \frac{1}{n}\ln c_e \tag{6}$$

where q_e and q_m (mg/g) are the equilibrium adsorption capacity and the maximum adsorption capacity, respectively; c_e (mg/L) is the equilibrium concentration of fluoride in the solution; K_L (L/mg) and K_F (mg/g) are the Langmuir and Freundlich adsorption constants, and n is related to the energetic heterogeneity.

The corresponding plots of c_e/q_e~c_e and lnc_e~lnq_e, as illustrated in Fig. 11, show the simulation results for fluoride onto the samples according to the Langmuir and Freundlich isotherm models. The related parameters obtained from linear regression by isotherm models are summarized in Table 2. It was observed that the correlation coefficients for Freundlich isotherm model ($R^2 > 0.99$) were higher compared to those for Langmuir model. Therefore, Freundlich isotherms can better fit to the experimental data with regard to fluoride adsorption on Al-doped Fe_3O_4/HAP nanocrystals at temperatures of 25°C, 35°C and 45°C, implying that the adsorption process involves multimolecular layers of coverage on a heterogeneous surface. Moreover, in all samples, the values of calculated 1/n are less than 1, which represents favourable conditions for fluoride uptake. To evaluate the thermodynamic feasibility and to confirm the nature of the adsorption process, the thermodynamic parameters including standard Gibbs free energy (ΔG), standard enthalpy (ΔH) and entropy change (ΔS) for the adsorption process were calculated using the following equation:

$$\Delta G = -RT\ln K \tag{7}$$

$$\Delta G = \Delta H - T\Delta S \tag{8}$$

where R is the universal gas constant (8.314 J/mol K), and T is the temperature in Kelvin (K). The calculated ΔG, ΔH and ΔS are displayed in Table 3. The negative values of ΔG and positive values of ΔH indicate that the fluoride sorption process is spontaneous and more favourable at higher temperature in nature. The positive ΔS values suggest the increase of randomness at the solid-solution interface during the fluoride adsorption process.

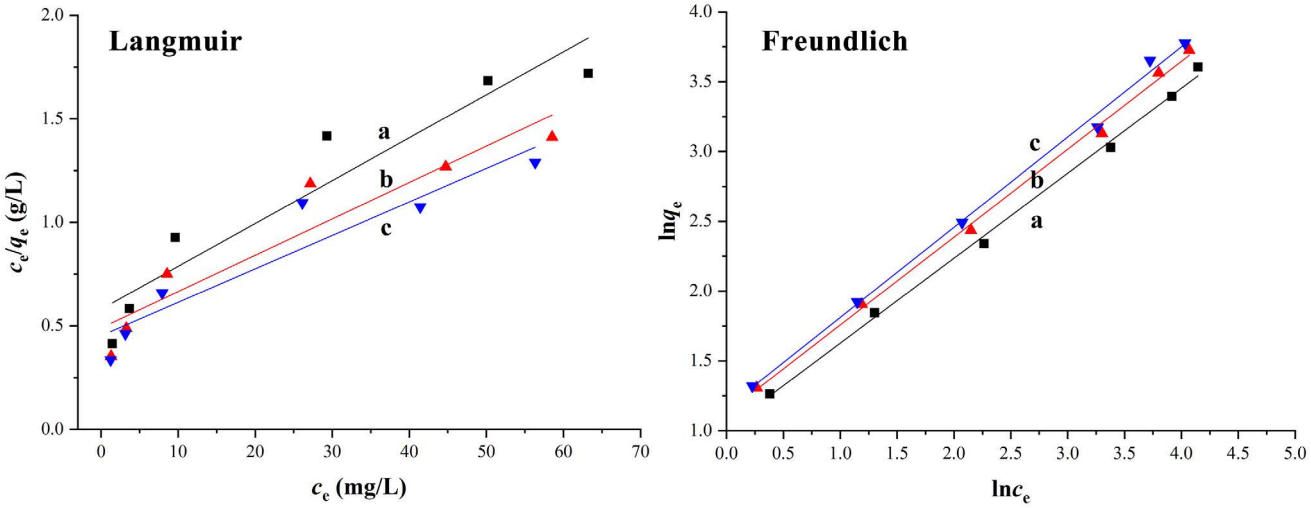

Fig. 11. Langmuir and Freundlich adsorption isotherm curves for fluoride on Al-doped Fe_3O_4/HAP nanocrystals (a) 25°C, (b) 35°C and (c) 45°C.

Table 2
Langmuir and Freundlich isotherm constants for adsorption of fluoride on Al-doped Fe_3O_4/HAP nanocrystals

Temperature (°C)	Langmuir			Freundlich		
	q_m (mg/g)	K_L (L/mg)	R^2	K_F (mg/g)	n	R^2
25	48.26	0.036	0.8806	2.768	1.643	0.9970
35	56.88	0.036	0.8697	3.090	1.589	0.9968
45	61.80	0.036	0.8628	3.207	1.548	0.9956

According to the discussion above, the scheme of the formation of Al-dope Fe_3O_4/HAP nanocrystals in pectin matrix and adsorption mechanism for fluoride is illustrated in Fig. 12. The pectin molecules act as stabilizer with specific functional groups can solve the problem of aggregation associated with magnetic nanoparticles in liquid media. The Al ions could be easily doped in the lattice of hydroxyapatite because of its small radii and high affinity to hydroxyl groups. Moreover, as a hard acid, Al ions have a high affinity to fluoride (hard base), and thus the Al doping benefits the fluoride adsorption. From the results of IR spectra, the doping of Al increased the content of hydroxyl group of hydroxyapatites, which could supply more ion-exchange sites for fluoride. Compared with Fe_3O_4/HAP, the doping of Al resulted in the larger isoelectric point value, which suggested strong electrostatic attraction exists between adsorbents and fluoride ions at a broader pH range. Finally, fluoride-loaded adsorbents were magnetically recovered by employing a strong external magnetic field.

4. Conclusions

In present study, the generation of Al-doped Fe_3O_4/HAP in pectin template via microwave-assisted method and its application as an adsorbent for removal of fluoride from aqueous solution are reported. The nanocomposites were synthesized with the iron salts co-precipitation followed by direct encapsulation with hydroxyapatite (HAP) and Al doping under microwave irradiation. The whole synthesis process of pectin-conjugated Al-Fe_3O_4/HAP nanocrystals was facile, rapid and environmentally friendly. During the formation of as-prepared sample, pectin molecules played a crucial role to control the morphology and size of Al-Fe_3O_4/HAP nanocrystals. This novel adsorbent combines merits of good magnetic separability and high affinity toward fluoride. Compared with pure HAP, the obtained Al-doped Fe_3O_4/HAP nanocrystals exhibited excellent adsorption capacity and rate for fluoride at ambient conditions through ion-exchange and high affinity of Al toward fluoride. The adsorption was predominantly the multimolecular layers adsorption of fluoride on a heterogeneous surface where both external and intraparticle diffusion contributed to the

Table 3
Thermodynamic parameters for fluoride adsorption on Al-doped Fe_3O_4/HAP nanocrystals

Temperature (°C)	ΔG (kJ/mol)	ΔH (kJ/mol)	ΔS (J/mol·K)
25	–15.81		
35	–16.72	11.34	91.12
45	–17.64		

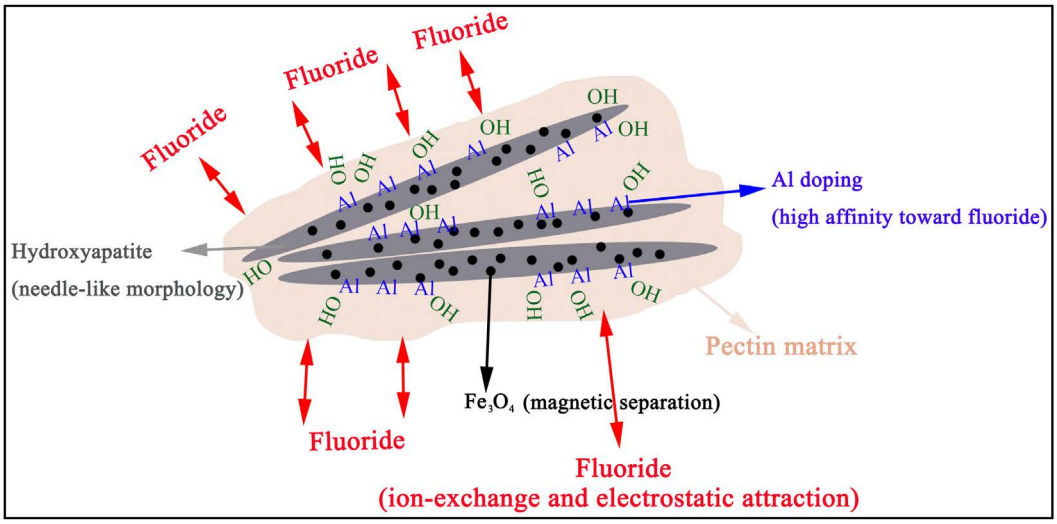

Fig. 12. Schematic diagram of Al-doped Fe_3O_4/hydroxyapatite adsorbents: high affinity toward fluoride with ease of magnetic separation.

rate of fluoride removal. Due to relatively high adsorption capacity and ease of magnetic separation, the Al-doped Fe_3O_4/HAP nanocrystals can be considered as a promising adsorbent for fluoride removal in water treatment.

References

[1] M. Levy, B.-S. Leclerc, Fluoride in drinking water and osteosarcoma incidence rates in the continental United States among children and adolescents, Cancer Epidemiol., 36 (2012) e83–e88.

[2] J. Fawell, K. Bailey, J. Chilton, E. Dahi, L. Fewtrell, Y. Magara, Fluoride in Drinking-Water, World Health Organization, IWA Publishing, London, 2006.

[3] C. Castel, M. Schweizer, M.O. Simonnot, M. Sardin, Selective removal of fluoride ions by a two-way ion-exchange cyclic process, Chem. Eng. Sci., 55 (2000) 3341–3352.

[4] D. Eunice Jayashree, G. Pooja, P. Senthil Kumar, G. Prasannamedha, A review on fluoride: treatment strategies and scope for further research, Desal. Water Treat., 200 (2020) 167–186.

[5] W. Kim, R. Singh, J.A. Smith, Modified crushed oyster shells for fluoride removal from water, Sci. Rep., 10 (2020) 5759, doi: 10.1038/s41598-020-60743-7.

[6] A. Abri, M. Tajbakhsh, A. Sadeghi, Adsorption of fluoride on a chitosan-based magnetic nanocomposite: equilibrium and kinetics studies, Water Supply, 19 (2019) 40–51.

[7] A. Bhatnagar, E. Kumar, M. Sillanpää, Fluoride removal from water by adsorption-a review, Chem. Eng. J., 171 (2011) 811–840.

[8] V.K. Gupta, D. Pathania, S. Agarwal, P. Singh, Adsorptional photocatalytic degradation of methylene blue onto pectin-CuS nanocomposite under solar light, J. Hazard. Mater., 243 (2012) 179–186.

[9] A. Behzadnezhad, T. Ebadi, S. Taheri, E. Kowsari, Batch adsorption of methyl tert-butyl ether (MTBE) from aqueous solution by combined CNT and zeolite, Desal. Water Treat., 191 (2020) 213–220.

[10] M. Al-Shannag, Z. Al-Qodah, M. Nawasreh, Z. Al-Hamamreh, K. Bani-Melhem, M. Alkasrawi, On the performance of *Ballota undulata* biomass for the removal of cadmium(II) ions from water, Desal. Water Treat., 67 (2017) 223–230.

[11] A. Sano, M. Takaoka, K. Shiota, Vapor-phase elemental mercury adsorption by activated carbon co-impregnated with sulfur and chlorine, Chem. Eng. J., 315 (2017) 598–607.

[12] D. Unlu, Recovery of cutting oil from wastewater by pervaporation process using natural clay modified PVA membrane, Water Sci. Technol., 80 (2019) 2404–2411.

[13] H. Agougui, M. Jabli, H. Majdoub, Synthesis, characterization of hydroxyapatite-lambda carrageenan, and evaluation of its performance for the adsorption of methylene blue from aqueous suspension, J. Appl. Polym. Sci., 134 (2017) 45385, doi: 10.1002/app.45385.

[14] L. Cui, L. Hu, X. Guo, Y. Zhang, Y. Wang, Q. Wei, B. Du, Kinetic, isotherm and thermodynamic investigations of Cu^{2+} adsorption onto magnesium hydroxyapatite/ferroferric oxide nanocomposites with easy magnetic separation assistance, J. Mol. Liq., 198 (2014) 157–163.

[15] J. Kim, N.S. Sambudi, K. Cho, Removal of Sr^{2+} using high-surface-area hydroxyapatite synthesized by non-additive in-situ precipitation, J. Environ. Manage., 231 (2019) 788–794.

[16] Y. Si, J. Huo, H. Yin, A. Wang, Adsorption kinetics, isotherms, and thermodynamics of Cr(III), Pb(II), and Cu(II) on porous hydroxyapatite nanoparticles, J. Nanosci. Nanotechnol., 18 (2018) 3484–3491.

[17] Z. Chen, Y. Liu, L. Mao, L. Gong, W. Sun, L. Feng, Effect of cation doping on the structure of hydroxyapatite and the mechanism of defluoridation, Ceram. Int., 44 (2018) 6002–6009.

[18] P. Mondal, D. Mehta, S. George, Defluoridation studies with synthesized magnesium-incorporated hydroxyapatite and parameter optimization using response surface methodology, Desal. Water Treat., 57 (2016) 27294–27313.

[19] P. Ramakrishnan, S. Nagarajan, V. Thiruvenkatam, T. Palanisami, R. Naidu, M. Mallavarapu, S. Rajendran, Cation doped hydroxyapatite nanoparticles enhance strontium adsorption from aqueous system: a comparative study with and without calcination, Appl. Clay Sci., 134 (2016) 136–144.

[20] J. He, K. Chen, X. Cai, Y. Li, C. Wang, K. Zhang, Z. Jin, F. Meng, X. Wang, L. Kong, J. Liu, A biocompatible and novelly-defined Al-HAP adsorption membrane for highly effective removal of fluoride from drinking water, J. Colloid Interface Sci., 490 (2017) 97–107.

[21] Y. Wang, L. Hu, G. Zhang, T. Yan, L. Yan, Q. Wei, B. Du, Removal of Pb(II) and methylene blue from aqueous solution by magnetic hydroxyapatite-immobilized oxidized multi-walled carbon nanotubes, J. Colloid Interface Sci., 494 (2017) 380–388.

[22] F. Xue, B. Wang, M. Chen, C. Yi, S. Ju, W. Xing, Fe_3O_4-doped lithium ion-sieves for lithium adsorption and magnetic separation, Sep. Purif. Technol., 228 (2019) 115750, doi: 10.1016/j.seppur.2019.115750.

[23] D. Bhardwaj, R. Singh, Green biomimetic synthesis of Ag–TiO_2 nanocomposite using *Origanum majorana* leaf extract under sonication and their biological activities, Bioresour. Bioprocess., 8 (2021) 1, doi: 10.1186/s40643-020-00357-z.
[24] W. Yang, X. Wu, Y. Dou, J. Chang, C. Xiang, J. Yu, J. Wang, X. Wang, B. Zhang, A human endogenous protein exerts multi-role biomimetic chemistry in synthesis of paramagnetic gold nanostructures for tumor bimodal imaging, Biomaterials, 161 (2018) 256–269.
[25] P.T.S. Kumar, C. Ramya, R. Jayakumar, S.K.V. Nair, V.K. Lakshmanan, Drug delivery and tissue engineering applications of biocompatible pectin-chitin/nano $CaCO_3$ composite scaffolds, Colloids Surf., B, 106 (2013) 109–116.
[26] J. Bok-Badura, A. Jakóbik-Kolon, K. Karoń, K. Mitko, Sorption studies of heavy metal ions on pectin-nano-titanium dioxide composite adsorbent, Sep. Sci. Technol., 53 (2018) 1034–1044.
[27] V.K. Gupta, D. Pathania, M. Asif, G. Sharma, Liquid phase synthesis of pectin–cadmium sulfide nanocomposite and its photocatalytic and antibacterial activity, J. Mol. Liq., 196 (2014) 107–112.
[28] N.V. Ivanova, N.N. Trofimova, V.A. Babkin, Larch bark pectinic polysaccharide as Ag (0) nanoparticle stabilizing matrix, Chem. Nat. Compd., 50 (2014) 60–64.
[29] K. Nigoghossian, M.V. Santos, H.S. Barud, R.R. Silva, L.A. Rocha, J.M.A. Caiut, R.M.N. Assunção, L. Spanhel, M. Poulain, Y. Messaddeq, S.J.L. Ribeiro, Orange pectin mediated growth and stability of aqueous gold and silver nanocolloids, Appl. Surf. Sci., 341 (2015) 28–36.
[30] L. Ai, Y. Zeng, Hierarchical porous NiO architectures as highly recyclable adsorbents for effective removal of organic dye from aqueous solution, Chem. Eng. J., 215–216 (2013) 269–278.
[31] X. Zhao, J. Wang, F. Wu, T. Wang, Y. Cai, Y. Shi, G. Jiang, Removal of fluoride from aqueous media by Fe_3O_4@$Al(OH)_3$ magnetic nanoparticles, J. Hazard. Mater., 173 (2010) 102–109.
[32] L. Gong, L. Feng, Preparation and defluorination mechanism of a novel copolymerized hydroxyapatite-aluminium chloride material, RSC Adv., 5 (2015) 95334–95343.
[33] Y.S. Ho, Review of second-order models for adsorption systems, J. Hazard. Mater., 136 (2006) 681–689.
[34] A. Phasuk, S. Srisantitham, T. Tuntulani, W. Anutrasakda, Facile synthesis of magnetic hydroxyapatite-supported nickel oxide nanocomposite and its dye adsorption characteristics, Adsorption, 24 (2018) 157–167.